Geometry assessment for a sloped type of wave energy converters

Gianmaria Giannini[a,b,*], Mario López[c], Victor Ramos[a,b], Claudio A. Rodríguez[d], Paulo Rosa-Santos[a,b], Francisco Taveira-Pinto[a,b]

[a]*CIIMAR - Interdisciplinary Centre of Marine and Environmental Research of the University of Porto, Terminal de Cruzeiros do Porto de Leixões, Avenida General Norton de Matos, S/N, 4450-208 Matosinhos, Portugal*
[b]*FEUP - Faculty of Engineering of the University of Porto, Department of Civil Engineering, rua Dr. Roberto Frias, s/n, 4200-465 Porto, Portugal*
[c] *DyMAST Research Group & Department of Construction and Manufacturing Engineering, University of Oviedo, EPM, C/ Gonzalo Gutiérrez Quirós s/n, 33600, Mieres, Asturias, Spain*
[d]*Laboratory of Ocean Technology (LabOceano), Department of Naval Architecture and Ocean Engineering, Federal University of Rio de Janeiro, Brazil*

*Corresponding author: gianmaria@fe.up.pt

Abstract

Oscillatory wave energy converters of the sloped type may allow absorbing power from ocean waves efficiently if a valid optimal design is used. In earlier studies, the optimized geometry for the CECO device was defined by implementing a simplified frequency-domain model. In this paper, that geometry is evaluated against the former one by taking into consideration a more realistic modelling approach and assessment scenario. The two geometries were benchmarked through a time-domain model, which allows taking into account realistic sea states and the use of end-stops to limit the amplitude of CECO motions. It was concluded that the optimized geometry allows extra energy production for most of the irregular sea states evaluated (45% more annual energy production). Performance indices were also used to compare the two geometries and it was concluded that the optimized geometry was particularly advantageous for the more energetic sea states. Overall, this study clearly shows that the choice of the generator rated power and end-stops span length are key aspects in determining realistically the annual energy production of sloped motion wave energy converters.

Keywords: ocean energy; WEC; efficiency; geometry optimization; oscillating body; numerical modelling.

This is a peer-reviewed, accepted author manuscript of the following article: Giannini, G., López, M., Ramos, V., Rodríguez, C. A., Rosa-Santos, P., & Taveira-Pinto, F. (2021). Geometry assessment of a sloped type wave energy converter. Renewable Energy, 171, 672-686. https://doi.org/10.1016/j.renene.2021.02.132

1. Introduction

High production of electricity from renewable energy resources is vital for allowing prosperous progress and sustainable growth. Due to land restrictions, conventional renewable energy resources, such as solar, onshore wind or freshwater hydropower could only satisfy a minimum part of the growing global energy demand. In contrast, marine renewable energy resources, such as offshore wind, wave and tidal energy, have an enormous global potential that could theoretically provide a reasonable share of usable energy to satisfy the world energy demand in future years. Different from tidal energy, which is limited to few coastal areas, offshore wind (already at a good stage of industrial development) and wave energy are the main resources that would allow increasing the differentiation of renewable energy production and energy self-sufficiency at coastal regions. Despite the enormous wave energy resource worldwide available [1], the total electricity produced from ocean waves, at present, is insignificant. The lack of wave energy industrial advancement is for the most due to a low technology readiness level leading to a high *Levelized Cost of Energy* (LCoE). Therefore, to progress a WEC technology, it is essential to optimize and validate the WEC design aiming at improving reliability and overall system performances for allowing viable LCoE plus reducing financial risks.

Starting from the last century numerous wave energy converters (WECs) concepts have been progressively proposed and developed [2]. The WEC technologies can be characterized in different ways, *e.g.* based on the type of power-take-off (PTO) system, location and principle of operation. Fig. 1 groups some examples of major WECs projects and categorizes these into two main clusters, Earth-reacting and self-reacting, and into three more subgroups, fixed structures [2-10], floating [11-20] and submerged [21, 22]. Fixed structures may be more suitable to be used for close-to-shore, based installations, for instance, installations in/or nearby harbours areas. Floating devices are appropriate for offshore locations where suitable water depths exist allowing mooring solutions to be cost-effective compared to fixed arrangements. Both floating and fixed devices can be completely submerged for reducing visual impacts and eventually for reducing peak structural loads during extreme storms. Compared to other options, conventional fixed structures might be more reliable and viable. As a matter of facts, fixed offshore wind turbines are already highly deployed compared to floating wind turbines, which instead are still at an initial stage of commercial progress. Similarly, it can be argued that fixed devices, for instance, the Wave Star [4] or CECO

[23] could be more viable, in the short-term, compared to other floating WECs.

Apart from structural aspects, the economic viability of WECs strictly depends on the PTO system employed. Various PTO types of systems exist, the most common ones are based on air turbines, hydraulic, direct electrical drive and mechanical systems [24]. For the oscillating type of WECs, direct drive or mechanical systems are the most suitable and reliable types, for instance, these are implemented respectively in the Power Buoy [15] and the CorPower [25] WECs. For simplicity at an initial stage of development, it may be opportune to consider the PTO as a linear mechanism assuming constant PTO damping coefficients C_{pto} that may be optimized based on wave climate conditions and WEC design for maximizing power absorption [26].

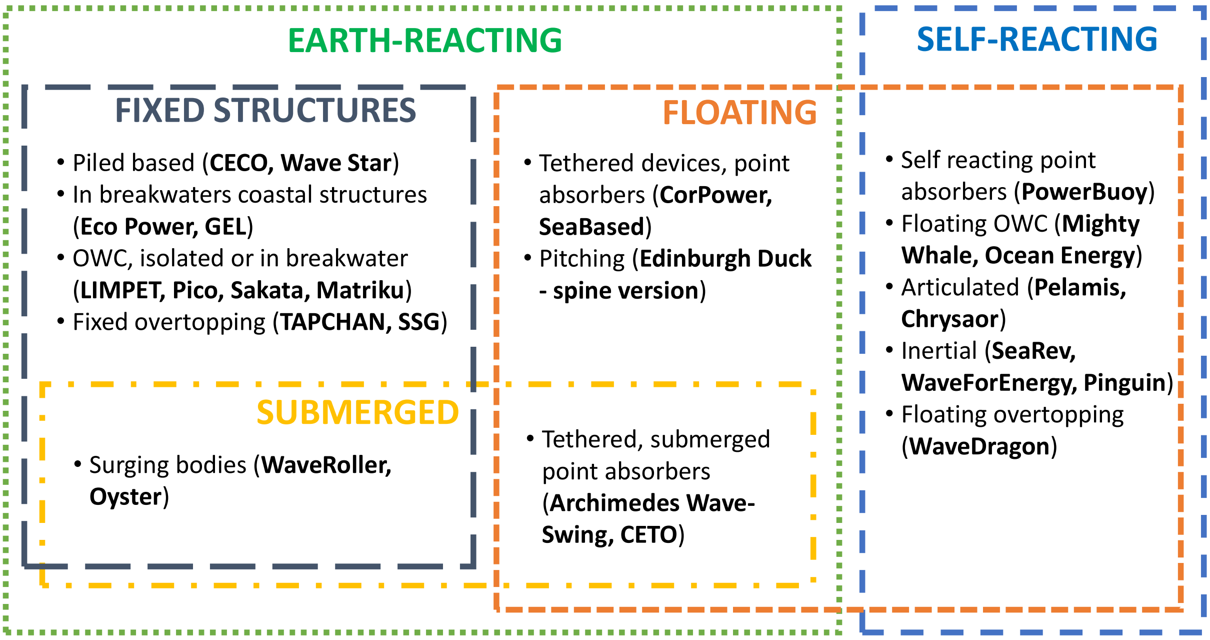

Fig. 1. Types of wave energy converters and examples.

In between the different types of WECs, a sloped motion type of oscillatory fixed WEC, as the CECO [3], may present advantages of higher system efficiency and minimal design characteristics. This type of WEC if correctly designed may allow good system response for maximizing power absorption and may not require extra expensive components for obtaining a reactive force needed for PTO operation. To authors' best knowledge any sloped motion fixed WEC was developed so far. Only a floating version of a sloped WEC was proposed by Salter [27]. In previous work, the CECO was developed by taking in consideration various factors such oscillating slope angle [28], depth of operation [29], wave climate [30] and, most importantly, the device geometry [26]. In fact, by implementing a frequency-domain based methodology, the floaters' geometry was optimized and initial results indicated that a significant increase in power production is expected [26]. However to validate this possibility further investigations are necessary, which would involve carrying out, experimental and, more advanced, time-domain based numerical studies.

For analysing the design of a sloped motion WEC including the PTO system, it is essential to use dynamic-based modelling methodologies. There is a vast range of different numerical modelling techniques and approaches [31]. These methods vary depending on the type of mathematical model involved, difficulty in implementation, computational costs and scope of use. In general terms, numerical modelling methods can be mainly subdivided in potential flow models (PFM), such as all those based on boundary element methods (BEM), and computation fluid dynamics (CFD) methods, based on Reynolds averaged Navier–Stokes (RANS) equations. PFMs are often applied by implementing hydrodynamic linearization assumptions and neglecting water viscosity. PFM involving only frequency-domain results do not capture transient dynamic effects thus often a time-domain approach based on Cummins equations [32] can be convenient. The main advantage of PFM is that they are computationally efficient; therefore, allow an analysis of a wide number of designs and environmental cases within feasible time. For example, during design optimization studies it may be required to analyse about thousands different WEC's geometries, which need to be assessed for several most recurrent sea states. On the other hand, PFM has some disadvantages such as low fidelity for large motions under extreme sea states due to linear assumptions. When PFM cannot be used it may be appropriate to employ CFD methods. While PFM is usually adopted during the initial stages of WECs development, CFD methods, that require conspicuous computational time, are better suitable during later stages to assess accurately particular factors such as extreme wave loads and power absorption estimates for a small number of specific sea states for which large WEC motions are expected and viscous forces are relevant.

Given the above reasoning, the present paper aims to assess the new geometry of CECO found by a frequency-domain methodology by implementing time-domain calculations based on PFM, which allows simulating the device more realistically also taking into account major dynamic effects and end-stops components that previously were neglected. The numerical analysis was carried out using an in-house developed Matlab code combined with the commercial software Ansys© Aqwa [33]. The new geometry is compared to the former one in terms of the dynamic response, power absorption performances relative to most important sea states and annual energy production. Given this scope, the paper, at first, covers a brief description of the CECO technology proposed (Sec. 2). An overview of initial proof-of-concept and experimental testing work is later briefly described (Sec. 3). Successively, the frequency and the time-domain numerical models for optimizing and analysing CECO are explained (Sec. 4) and details of CECO versions analysed are provided. Finally, the main results and general aspects are covered (Sec. 5) and the main conclusions are drawn (Sec. 6).

2. The CECO technology

CECO is an oscillatory type of WEC that, differently from usual heaving or pitching devices, oscillates along an inclined direction of motion [3, 23, 34]. The CECO device consists of a fixed central support structure, Fig. 2 (a). Inside the support structure, the electric generator is allocated. The generator is actuated by the motion of a sliding frame, which rigidly connects the two lateral mobile modules (LMMs). The inclined direction allows for the absorption of the wave energy from a combination of heave and surge. By decreasing the angle of inclination (Fig. 2 b) the natural response of the device increases. The translational motion is converted into rotation with a rack-pinion system [23], which is composed of a generator and rack elements located, as for Fig. 2 (a). The LMMs, together with the connecting frame, translates between upper and lower end-stops (Fig. 2 a), which limit the excursion of the sliding frame.

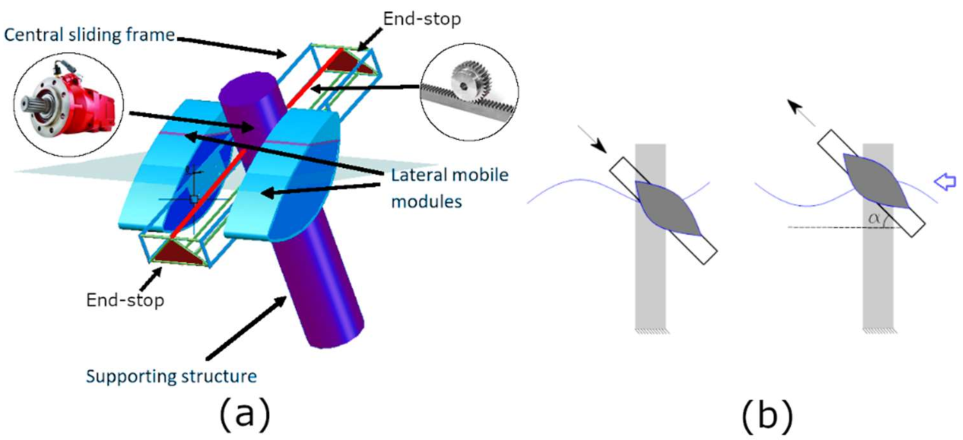

Fig. 2. (a) CECO main components, (b) CECO working principle.

The CECO design was developed over recent years by investigating the most significant parameters and by improving the geometry of the LMMs. The effects of power-take-off (PTO) damping values [35] and sliding angles [28] were investigated in separate occasions. In particular, it was found that the sliding angle might be adjusted to improve significantly the performances given a specific wave climate. At Portuguese offshore locations, it was found that optimal sliding angles should be in the range of 30-45° [28]. Recently, the geometry of LMMs was optimized by investigating various possible shapes [26]. These geometries were defined and systematically assessed with a model based on a frequency-domain approach. A slender type of LMMs (Fig. 3 a) showed to perform significantly better than the former half-cylinder shaped LMMs (Fig. 3 b). The optimal choice of mass, cross-sectional area (depending on geometry and mass) and the sliding angle allows tuning the device for a recurrent sea state aiming to resonance condition, thus increasing power absorption.

3. Proof-of-concept and numerical model validation

To validate the CECO concept and the PFM approach applied to this kind of WEC, a series of experimental campaigns were carried out. The main objective concerned of preliminary validate calculations and confirm, at model scale, that the CECO device would suit typical wave climates relative to the west coast of the Iberian Peninsula, which have consistent energy densities within the range of wave periods of 10 to 15 s and wave heights of 1 to 5 m. The experimental work was performed in the ocean basin of the Faculty of Engineering of the University of Porto (28.0 m long, 12.0m wide and 1.2 m deep) using mono-directional, regular and irregular, sea states. Experimental investigation of two simplified CECO model-scale devices was carried out. The former geometry was evaluated by constructing a model at a scale of $\lambda = 1{:}20$, Fig. 3. Successively, a second CECO model was defined, in particular, by varying the LMMs shape [26]. The optimized LMMs, that are shown in Fig. 3 (b), were later tested at $\lambda = 1{:}25$. As anticipated, the firsts LMMs had a shape of a half-cylinder and the optimized LMMs are of a slender shape. In both circumstances, a frame (Fig. 3 (a), side view), was connecting the two LMMs and driving a simplified PTO, which consisted of a rack-pinion system with an electric generator. For varying the PTO damping values, a circuit was implemented that allowed to apply different electric resistances. Besides changing PTO damping values also various PTO inclinations (sliding angle) were investigated.

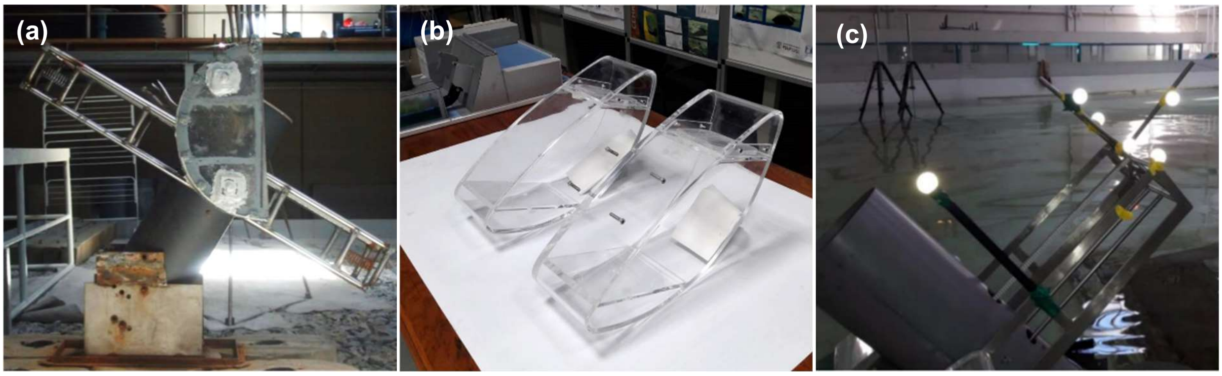

Fig. 3. CECO physical models, where (a) has the initial LMMs, (b) the optimized LMMs and (c) is the CECO model setup in water.

Both the LMMs motions and the power output were measured, and following Froude scaling laws, converted to full-scale quantities. The LMMs motion was monitored through the Qualysis® motion capture system by installing markers on the models, as shown in Fig. 3 (c). Through direct and indirect analysis methods, the PTO forces and the power absorbed can be estimated. In all cases, before experiments in water, the electric generator was calibrated through weight drop tests. For characterizing different PTO loads, a range of resistances between 10 to 100 Ω was assessed.

The experimental results proved the functioning of the concept and, as well, its potential in terms of performances. Regular and irregular sea states test results confirmed high-efficiency values of the CECO in absorbing wave power for both geometries. With sea states of T_p in the range 8 to 12 s and H_s of 1 to 3 m the CECO efficiency η (*mean device kinetic power/mean sea state power*) can be between 0.15 up to 0.55 [36] when suitable C_{pto} values are used.

The data acquired in early experimental investigations allowed proving the CECO concept and to do an initial numerical model validation. On the other hand, due to the experimental scale used, empirical results alone may not allow comparing the two geometries assessed with accuracy. Thus, for the scope of the study, a numerical investigation is more appropriate.

4. Numerical modelling

Numerical modelling of WEC comprehends structure-independent wave resource modelling, frequency-domain and time-domain models, which instead relate to the fluid-structure interaction hydrodynamics problem.

4.2.Wave resource modelling

A comparative analysis for the former and optimized LMM geometry of CECO was conducted against the energetic wave conditions of the pilot zone of San Pedro de Moel (Portugal), which spans a total surface of 400 km^2, with water depths ranging from 20 to 90 m. The wave conditions of the region were characterised for an 11-year horizon (from 2005 to 2015) by means of the spectral wave model SWAN [37, 38]. For this purpose, the offshore wave conditions were propagated towards the Portuguese coast. The aforementioned offshore wave conditions were acquired from the SIMAR-44 hindcast data sets (Spanish State Port Authority), which are obtained through numerical modelling by coupling both a high-resolution atmospheric model REMO [39] and the spectral wave model WAM [40]. For further details on the implementation and validation of the spectral wave model, the readers can refer to [30] and [29]. Then the computed nearshore wave conditions were used to construct the omnidirectional wave energy matrix for a specific location within the pilot zone (Fig. 4), with the sea states characterised in terms of significant wave height, H_s, peak wave period, T_p, the annual number of hours of occurrence, h_i, and omnidirectional wave energy, E_{Wi}, Fig. 4. The energy resource is located for the most within the H_s range of 1-5 m and T_p of 4 to 18 s. As can be seen in Fig. 4, sea states with wave heights above 7.5 m are rare (only 1 hour of occurrence per year) thus for the scope of the study other sea states with higher H_s were not considered.

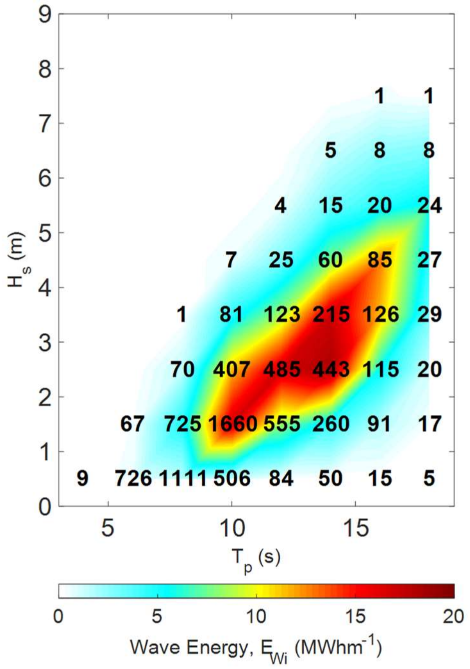

Fig. 4. Wave energy resource matrix for São Pedro de Moel, Portugal (39° 49′ 12″ N, 9° 03′ 36″ W). Numbers represent hours of occurrence.

4.3.Frequency-domain model of the CECO device

Despite the simplifying linear assumptions, frequency-domain modelling of the CECO device is highly desirable for the initial assessment of WEC performance. However, since most of the available numerical tools for the computation of hydrodynamic coefficients and motions only provide direct output relative to the classical ship's six rigid-body degrees of freedom, the prediction of the hydrodynamic behaviour for inclined degrees of freedom involves further challenges.

Sarpkaya [41] provides expressions for the computation of hydrodynamic coefficients derived by Sedov [42] for 2D floating structures rotated with respect to a Cartesian-reference system. Based on those expressions, it is possible to estimate added mass, damping and hydrostatic coefficients for the inclined degree of freedom using the results from the surge and heave modes. Then, the equation of motion of the inclined mode can be written as a single-degree-of-freedom equation that can be easily solved. It should be noted that depending on the underwater shape of the floater, Sedov's expressions could be a good approximation for 3D geometries. An alternative approach is to use a hydrodynamic code able to deal with generalized modes, for instance, Wamit® [43]. In this last code, the inclined direction can be defined as an additional (generalized) mode so that the solution of the 3D radiation-diffraction hydrodynamic problem can be directly solved.

The assessment of the former shape of CECO's LMMs and the search of the optimized geometry has been performed with the aid of Wamit® (further details on the adopted frequency-domain model and the optimization process are described in [26]). The effects of inclination, water depth and submergence of LMMs have been numerically investigated using both the former and the optimized CECO's LMMs geometries. The natural oscillation period is affected by the inclination angle of the motion path. CECO inclinations between 15° and 60° allow achieving natural periods between 20 s and 5 s, respectively, i.e. within the range of typical peak periods of most worldwide sea states. Since the selected target sea state is characterized by 1.5 m of significant wave height and 10 s of the peak period (Fig. 4), the PTO inclination was set to 30°. In this way, the CECO's resonance is achieved during most of its annual operation.

The RAOs of the former and optimized geometries for the 30° inclination are shown in Fig. 5 for several values of linear (external) PTO damping, where viscous effects and other losses have not been accounted for. For the 30° inclination, the natural periods of both geometries are quite close; however, the differences between the WEC designs start to appear in the amplitudes of motions, especially around the WEC's resonance periods.

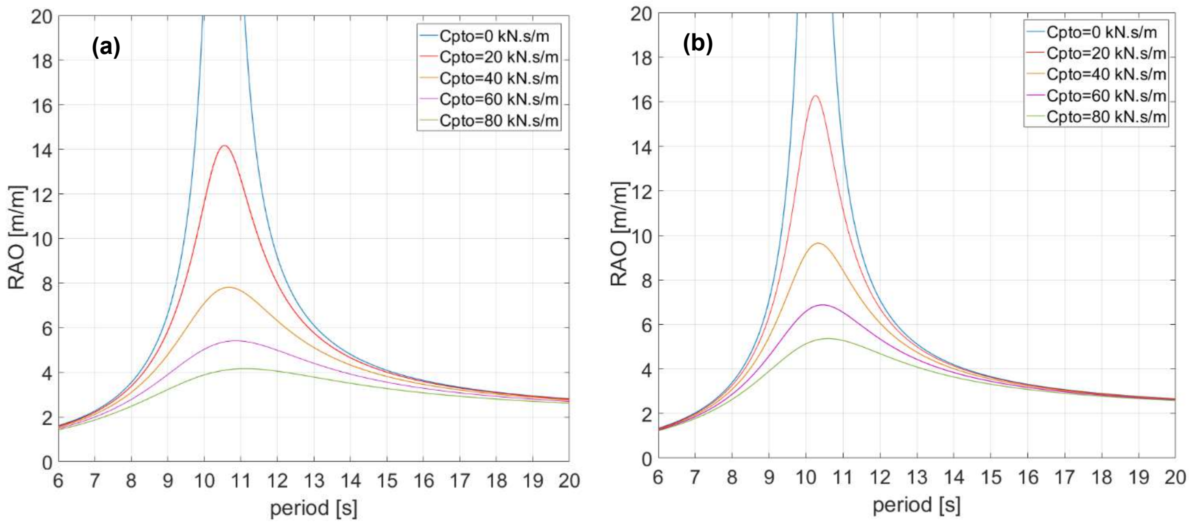

Fig. 5. Response amplitudes under regular waves for the 30° and several linear PTO damping values (frequency-domain model): (a) former geometry (b) optimized geometry

Following the derivations presented by Falnes [44], the optimum PTO damping and the absorbed power can be easily obtained for regular wave conditions. However, for stochastic seas, both the optimum PTO damping and the associated maximum absorbed power cannot be computed from analytical expressions. However, Rodríguez et al. [26] have proposed a definition for the maximum absorbed power in stochastic seas based on the superposition principle typically adopted for the description of irregular seas. The idea behind that definition is to assume that for each regular wave-component (that composes a given irregular sea) its corresponding optimum PTO damping coefficient is applied so that maximum power can be absorbed from it. In other words, the maximum (or "ideal") absorbed power from a given sea state is the superposition of the theoretical maximum absorbed power from each of its wave components. In terms of Falnes' [44] nomenclature, the optimum amplitude condition is satisfied for every (regular) wave component, except for the one that matches the WEC's natural period where the optimum phase condition is also satisfied. Therefore, to compute the power absorbed from each component of an irregular wave spectrum, the maximum absorbed power per square wave amplitude as a function of (regular) wave period (Fig. 6 b) should be multiplied by the respective square amplitudes of the components of the sea spectrum. The integration of those "regular-wave powers" provide the maximum or "ideal" power that could be absorbed by the given sea state.

Fig. 6a presents the theoretical (regular wave) optimum damping values used to obtain the corresponding power functions (kW/m^2) reported in Fig. 6 b. Both functions are independent of the sea spectrum. As expected from the theoretical expressions given by Falnes [44], the peak of the function of absorbed power occurs at the natural frequency of the WEC motion for the respective WEC geometries. Although the peak of the power of the former CECO is slightly larger than the optimized CECO, the latter is broader than the former and presents a PTO damping coefficient function that is significantly higher, especially for the wave periods above resonance. This feature is desirable since, for later analyses, part of the theoretical PTO damping should be deducted to account for unavoidable (mechanical, electrical, viscous, etc.) losses. Then, only the remaining part of the theoretical PTO damping can be considered as useful power absorption.

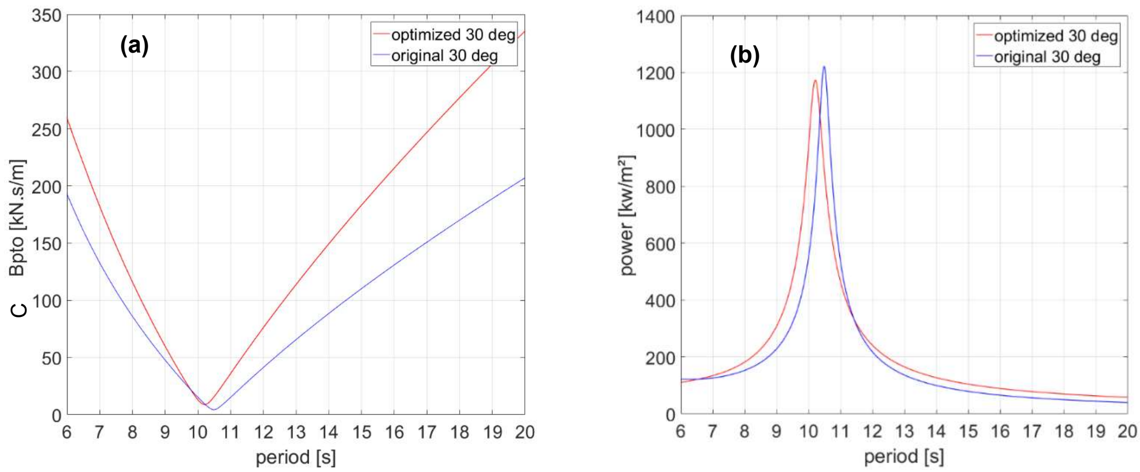

Fig. 6. Optimal PTO damping coefficients (a) and power functions (b) obtained from frequency-domain analysis in regular waves.

The power absorbed from each (regular wave) component that forms the sea spectrum of the target sea-state (JONSWAP spectrum) for the former and optimized CECO at the 30° inclination, for several PTO damping coefficients, is shown in Fig. 7. Here, the improved performance of the optimized geometry over the former design is evident, especially when higher PTO damping coefficients are adopted. Based on systematic variations of (constant) PTO damping for the target sea-state, the absorbed power corresponding to each PTO variation has been computed, and a maximum value has been identified.

The PTO damping coefficient corresponding to the maximum absorbed power at the target sea-state for the 30° inclination has been regarded as the best PTO damping coefficient (C_{opt}). As for the regular wave conditions, the C_{opt} of the optimized CECO resulted higher than the C_{opt} of the former geometry. In terms of absorbed power, the optimal C_{opt} provided 80.31 kW for the former CECO and 100.74 kW for the optimized geometry. Thus, representing an improved performance of around 25% for the optimized geometry over the former design.

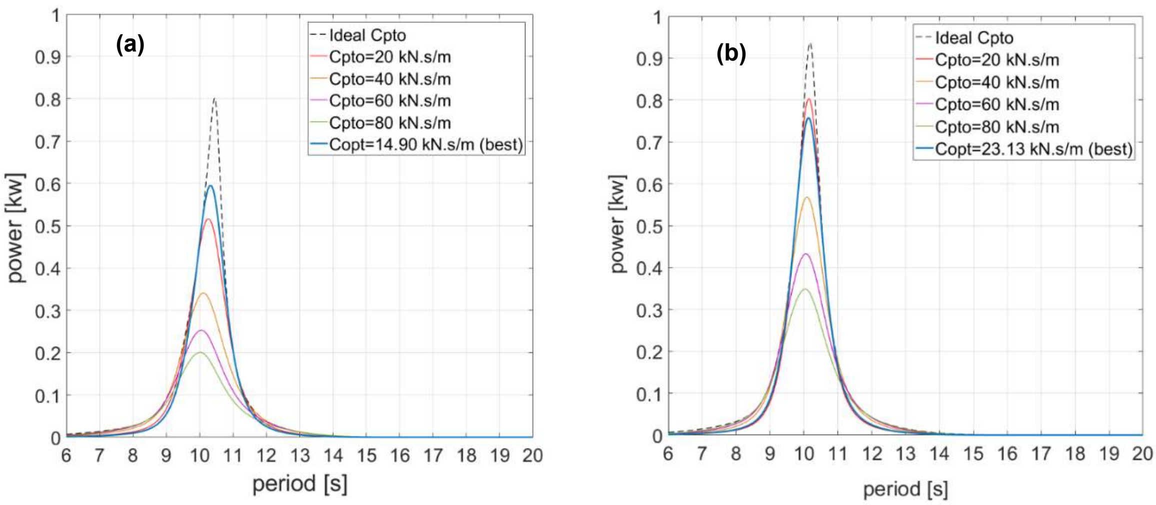

Fig. 7. Power absorbed for each component of the target sea state (JONSWAP spectrum, T_P=10 s, H_S=1.5 m), 30° motion inclination and different PTO damping values: (a) former geometry and (b) optimized geometry.

The linear frequency-domain modelling has allowed performing and gaining valuable insight into the hydrodynamic behaviour and power assessment of both WEC designs. Furthermore, it has shown to be very computationally efficient. However, to verify if the linear assumptions inherent to the frequency-domain model are valid, nonlinear time-domain simulations need to be performed for both CECO geometries.

4.4.Time-domain model

The behaviour of CECO in irregular wave conditions can be analysed in the time-domain by using a potential flow model and including instantaneous forces. First, the source distribution method needs to be used to obtain the flow potential (φ), which is the superposition of the undisturbed incident potential (φ_I), the diffraction potential (φ_d), and the radiation potential (φ_r). Bearing in mind that the wetted surface of the LMMs changes significantly during operation, the free surface position is re-evaluated in each time step of the simulation to compute the instantaneous hydrostatic and hydrodynamic forces. This approach allows including some nonlinearities that the frequency domain linear model cannot reproduce (linear models assume small motion amplitudes incompatible with the large displacements of the LMMs under high energetic wave conditions). For this purpose, the total surface of the LMMs was meshed and not only the wetted surface below the mean water level – which is used to compute the diffraction and the radiation force components (Fig. 8). For the former geometry, 968 panels were used (of which 552 diffracting panels). Differently, for the optimized version, 1539 panels were used (of which 877 diffracting).

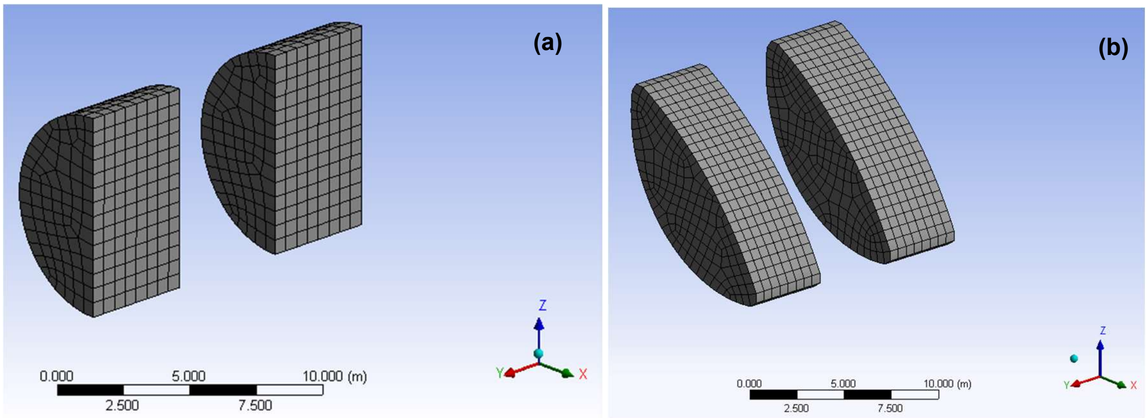

Fig. 8. Meshes used for former (a) and optimized (b) LMMs geometries.

Being **M** the structural mass matrix of the floating part of CECO, and **x** = (x,y,z) its displacement vector from its hydrostatic equilibrium (with components corresponding to x, surge; y, sway; and z, heave; Fig. 8), the numerical approach can be described with the following equation of motion:

$$\mathbf{M}\ddot{\mathbf{x}} = \mathbf{F}_{HS} + \mathbf{F}_{FK} + \mathbf{F}_{D} + \mathbf{F}_{R} + \mathbf{F}_{M} + \mathbf{F}_{PTO} \quad (1)$$

where, $\mathbf{F}_{HS}$ is the hydrostatic force under the instantaneous wetted surface of the LMMs, $S(t)$, which is given as the balance between the gravity force and the Archimedes force at each time step in a simulation:

$$\mathbf{F}_{HS}(t) = \mathbf{F}_{G}(t) + \int_{S(t)} p_{st}(t)\mathbf{n}dS \quad (2)$$

where $\mathbf{F}_G$ is the gravity force, $p_{st}(t) = -\rho g z(t)$ the instantaneous static pressure, and n a vector normal to the surface. In this last formula, ρ is the water density, g the gravitational constant and $z(t)$ the vertical displacement changing with time.

$\mathbf{F}_{FK}$ is the hydrodynamic Froude–Krylov force under the instantaneous incident wave surface,

$$\mathbf{F}_{FK}(t) = -\int_{S(t)} p_{dyn}(t)\mathbf{n}dS \quad (3)$$

where $p_{dyn}(t)$ is the hydrodynamic pressure obtained by applying Wheeler stretching method [45].

$\mathbf{F}_D$ is the diffraction force contributed by all the diffracting panels (i.e. those below the mean water level),

$$\mathbf{F}_D(t) = -\int_{S_0} p_d(t)\mathbf{n}dS \tag{4}$$

where $p_d(t)$ is the diffraction wave pressure (quadratic terms are neglected), which is integrated over the mean wetted surface (S_o) of the LMMs.

$\mathbf{F}_R$ is the radiation force consisting of the impulse function convolution, which accounts for the past motion of CECO, so-called "memory effect" [32], and the hydrodynamic inertia force or added mass at the infinite frequency ($\mathbf{A}_\infty$),

$$\mathbf{F}_R(t) = -\mathbf{A}_\infty\ddot{\mathbf{x}}(t) - \int_0^t \mathbf{h}(\boldsymbol{t}-\tau)\ddot{\mathbf{x}}d\tau \tag{5}$$

with

$$\mathbf{h}(t) = \frac{2}{\pi}\int_0^\infty \mathbf{B}(\omega)\frac{\sin(\omega t)}{\omega}d\omega = \frac{2}{\pi}\int_0^\infty \{\mathbf{A}(\omega) - \mathbf{A}_\infty\}\cos(\omega t)\,d\omega \tag{6}$$

where $\mathbf{B}(\omega)$ and $\mathbf{A}(\omega)$ are the added mass and hydrodynamic damping matrices,

$$\mathbf{A} = \frac{\rho}{\omega}\int_{S_0} \mathrm{Im}(\varphi_r)\mathbf{n}dS \tag{7}$$

and

$$\mathbf{B} = -\rho\int_{S_0} \mathrm{Re}(\varphi_r)\mathbf{n}dS \tag{8}$$

where φ_r is the radiation velocity potential.

$\mathbf{F}_M$ is the summation of the fluid forces acting on the slender elements of CECO (the tubes of the frame between both LMMs), which can be computed by integrating over the wetted length of each tube the cross-sectional Morison's force [46] defined as

$$d\mathbf{F}_M = \frac{1}{2}\rho\phi_D C_D|u_f - u_s|(u_f - u_s) + \rho\phi_A C_m\dot{u}_f - \rho\phi_A(C_m - 1)\dot{u}_S \tag{9}$$

where ϕ_D is the characteristic drag diameter, C_D is the drag coefficient, u_f and $\dot{u}_f$ are the transverse directional fluid particle velocity and acceleration, u_s and $\dot{u}_S$ the transverse directional structure velocity and acceleration, C_m is the inertia coefficient and ϕ_A the cross-sectional area.

$\mathbf{F}_{PTO}$ is the PTO force, which accounts for the forces in the conversion machinery that oppose the motion (e.g., friction losses, electromotive forces, and mechanical losses),

$$\mathbf{F}_{PTO}(t) = -\left[f + C_{PTO}\dot{\xi}(t)\right]\mathbf{e} \tag{10}$$

where $\dot{\xi}$ is the translation speed of the CECO floating part, f a friction force for $\dot{\xi}$, C_{pto} a damping coefficient that takes different values and $\mathbf{e}$ a unit vector that defines the direction of the PTO axis with respect to the global axes.

The motion of the LMMs and the inner frame is constrained by upper and low end-stops. For the correct modelling of CECO, these limits need to be considered into calculations. To note that considering such limits is only possible with the implementation of a time-domain approach. The end-stops can be modelled as units having spring and damping properties. The force induced by an end-stop can be estimated as:

$$\mathbf{F}_{FEN} = -[K_{es}\Delta Y + C_{es}\dot{\xi}(t)]\mathbf{e} \tag{11}$$

where K_{es} is the spring stiffness, ΔY the compression length of the end-stop, and C_{es} the damping value. The coefficient C_{es} can be quantified by kinetic energy considerations:

$$E = 0.5\, m \left|\dot{\xi}(t)\right|^2 C_m \tag{12}$$

where m, V and C_m are the mass, velocity and added mass coefficient of the LMMs. Each time the LMMs reach their higher or lower limit of operation, during contact with the end-stop, part of the kinetic energy is lost, as for:

$$E_1 = E_2 - E_{loss} \tag{13}$$

where E_1 is the initial kinetic energy, E_2 the remaining kinetic energy after hitting the end-stop and E_{loss} the energy dissipated during the contact. E_{loss} can be set equal to λE_1, where λ is a dissipation coefficient. The fixed damping parameter C_{es} can then be estimated using:

$$C_{es} = \frac{E\,\lambda}{\left|\dot{\xi}(t)\right|^2 T} \tag{14}$$

where T is the contact period between the moving body and the end-stop.

The time-domain calculations were carried out with the aid of the commercial software Ansys© Aqwa [33] and an in-house developed Matlab code. A predictor-corrector integration scheme is used. During the first stage, all forces on the device's floating part at time t (as functions of time, position and velocity) are calculated. Subsequently, the body acceleration is obtained, and the velocity and the position are predicted at the next time step, $t + \Delta t$. At a second stage, the applied forces are recalculated at time $t + \Delta t$, and the values of the velocity and position corrected by using Taylor's theorem. For more details on the mathematical theory implemented the reader can refer to [32, 33, 47].

4.5. CECOs physical parameters

To compare the former CECO geometry with the optimized one, specific system parameters were selected given findings of prior studies based on a frequency-domain analysis [26]. The two CECO designs varied essentially in terms of the LMMs shape, dimensions, draft and mass values. All other factors, such as the PTO sliding angle, overall width, supporting structure and frame dimensions, were set to be the same for both designs, Table 1. A sliding inclination angle equal to 30° was adopted, as this value showed to have the best efficiency for the recurrent sea states of the coastal area in the study [28]. In Fig. 9 are reported the dimensions in meters of the CECO version analysed. The main differences between the two CECO designs are the mass and the wetted surface of the LMMs. Both these values are higher for the optimized geometry.

Table 1. Parameters of a single former and optimized lateral mobile module (LMM).

Parameter	Former LMM	Optimized LMM
PTO inclination angle (°)	30°	30°
Overall length (m)	4	10
Overall width (m)	4.5	4.5
Overall height (m)	8	10
Draught (m)	4.61	5.25
Mass, m (t)	69	179

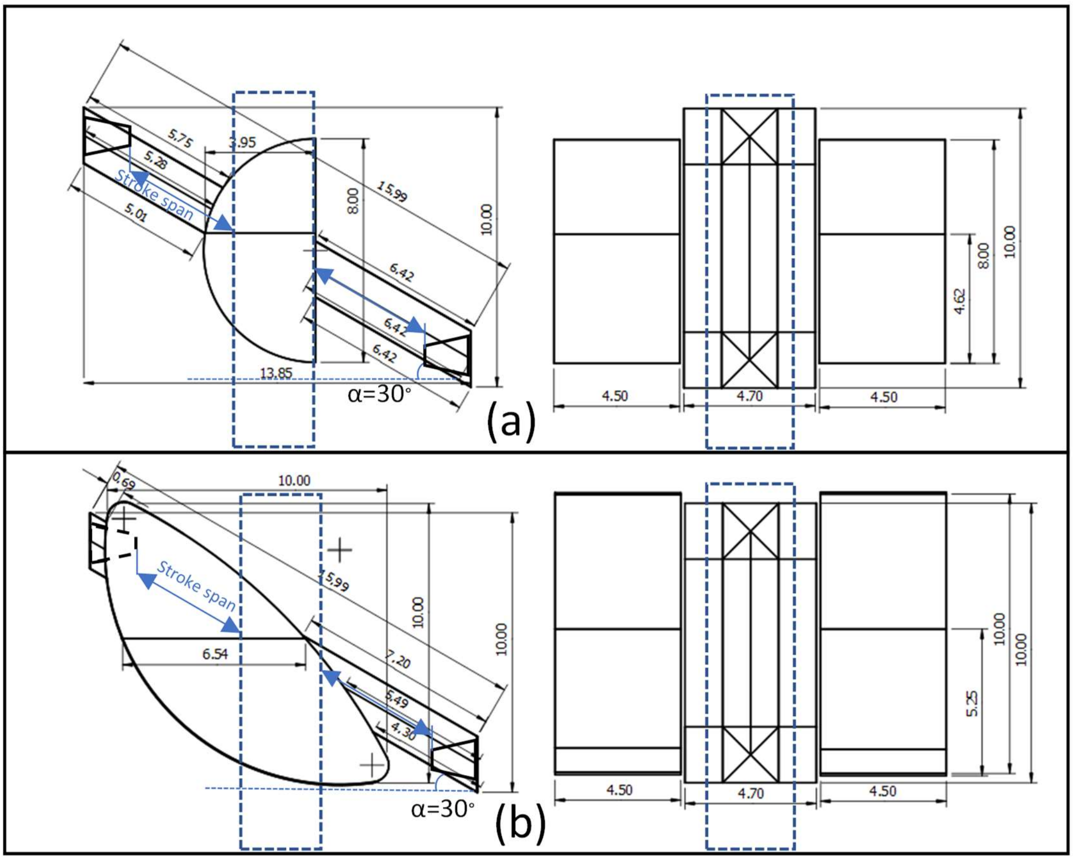

Fig. 9. Dimensions (in meters) of LMMs and sliding frame of former (a) and optimized (b) CECOs.

5. Results

The two geometries were analysed and compared in terms of hydrodynamic coefficients, natural periods, time-domain time series, power matrices and energy production performances.

5.1. Added mass, radiation damping and excitation forces coefficients

The hydrodynamic parameters characterizing the two geometries need to be at first calculated. For surge and heave components, Fig. 10 shows the added mass coefficients (a,b), the radiation damping coefficients (c,d) and the wave excitation forces (e,f). By comparing the former (dotted blue line) with the optimized geometry (red line), it is noticed that the magnitude of the added mass, radiation damping coefficients and wave excitation forces are comparable for both geometries only for what concerns the surge components (index 11). Differently, for the optimized geometry the heave related quantities, coefficients are significantly higher (Fig. 10 b,d,f).

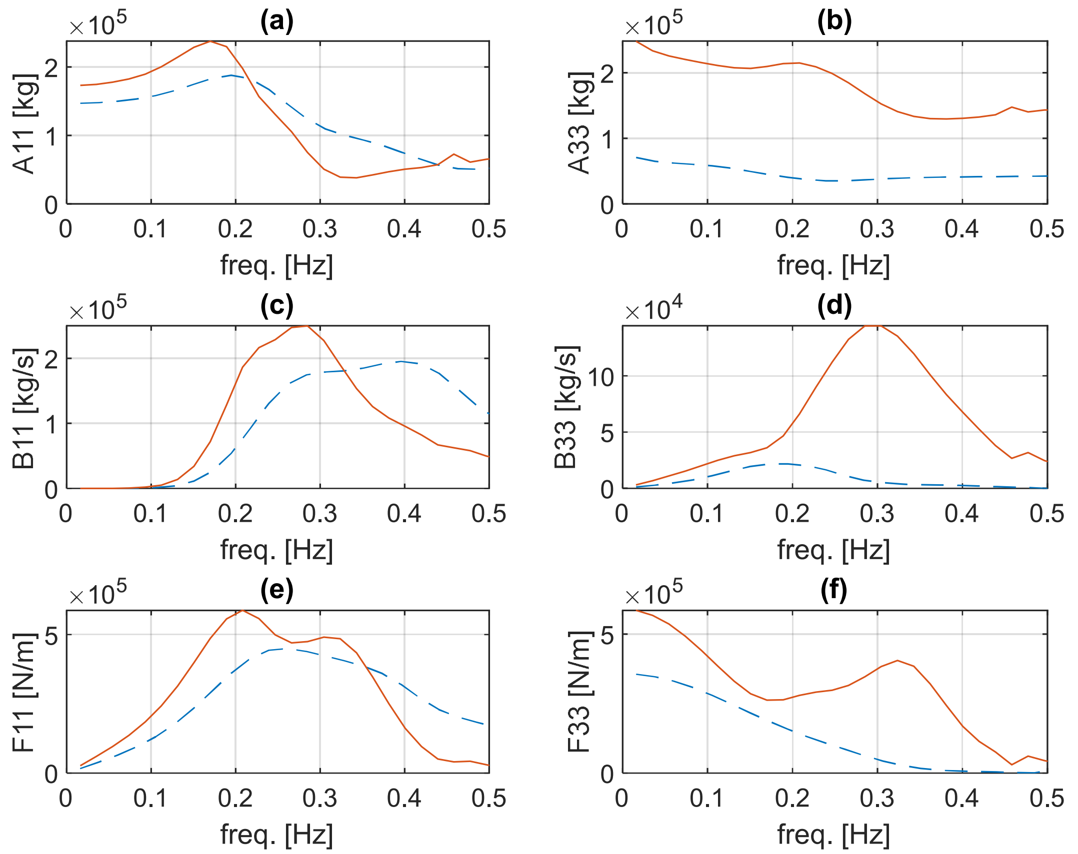

Fig. 10. Hydrodynamic coefficients of former (dashed lines) and optimized (continues line) LMMs: (a) surge and (b) heave components of the added mass; (c) surge and (d) heave components of the radiation damping; (e) surge and (f) heave wave excitation forces per unit of wave amplitude (Froude-Krylov and diffraction).

5.2. Time-domain analysis results

The hydrodynamic coefficients allowed solving the equation of motion of CECO in the time-domain. The natural period of the response of CECO was obtained with numerical free-decay oscillation tests using the time-domain model. These tests can be performed by assuming an initial offset of the device from the equilibrium position, at the starting time (t = 0) and no waves. Both CECO geometries were evaluated for 30°, 45°, 60° and 90° of PTO inclinations. Despite the differences in terms of hydrodynamic parameters for the two geometries, the obtained natural periods are similar, Fig. 11. Regardless of the higher mass of the optimized LMMs, the particular slender shape coupled with the direction of motion and higher cross-sectional area determines natural periods to be similar.

As shown in Fig. 11, time-domain results of natural periods are well in agreement with frequency-domain results.

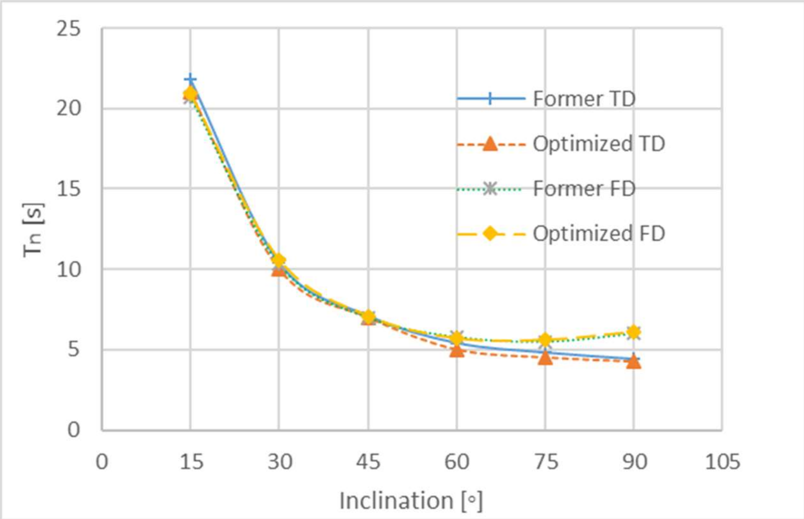

Fig. 11. The natural period of oscillation T_n as a function of the inclination. Results for former and optimized geometries obtained with time-domain (TD) and frequency-domain (FD) calculations.

Numerical simulations were run for the 45 most relevant irregular sea states, following the wave resource matrix previously introduced (Fig. 4). For illustration, Fig. 12-Fig. 14 show results for the two most energetic sea states (Hs = 1.5 m, Tp = 10 s and Hs = 2.5 m, Tp = 14 s) and a severe sea state (Hs = 7.5 m, Tp = 16 s). It can be noted that for the recurrent sea states (Fig. 12 and Fig. 13), the optimized CECO geometry has similar motions and peak velocities. However, the power absorbed by the optimized geometry is higher. In all cases, the optimized CECO reaches the rated power value, which for simplicity was initially set at 0.5 MW. A higher value of rated power would be beneficial, in particular, for the optimized geometry. For what concerns the severe state time series illustrated, the power output of both, former and optimized CECOs, is more similar (Fig. 14) because the rated power limit is reached by both geometries for almost all the waves.

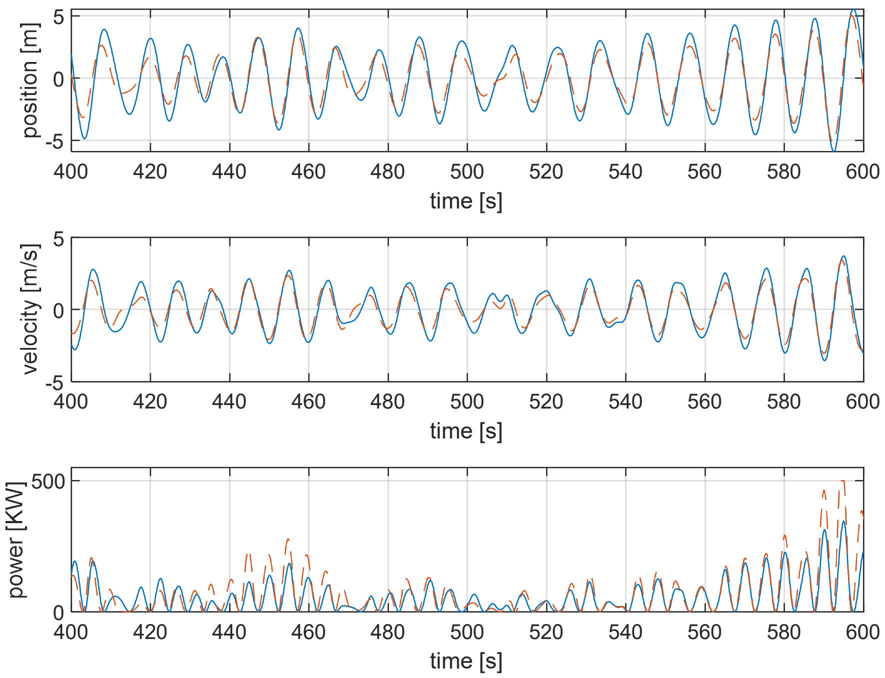

Fig. 12. Irregular sea state time series related to Hs=1.5 m and Tp = 10 s. Former CECO @25 kNs/m results and optimized CECO @50 kNs/m are depicted respectively by blue and red (dotted) line.

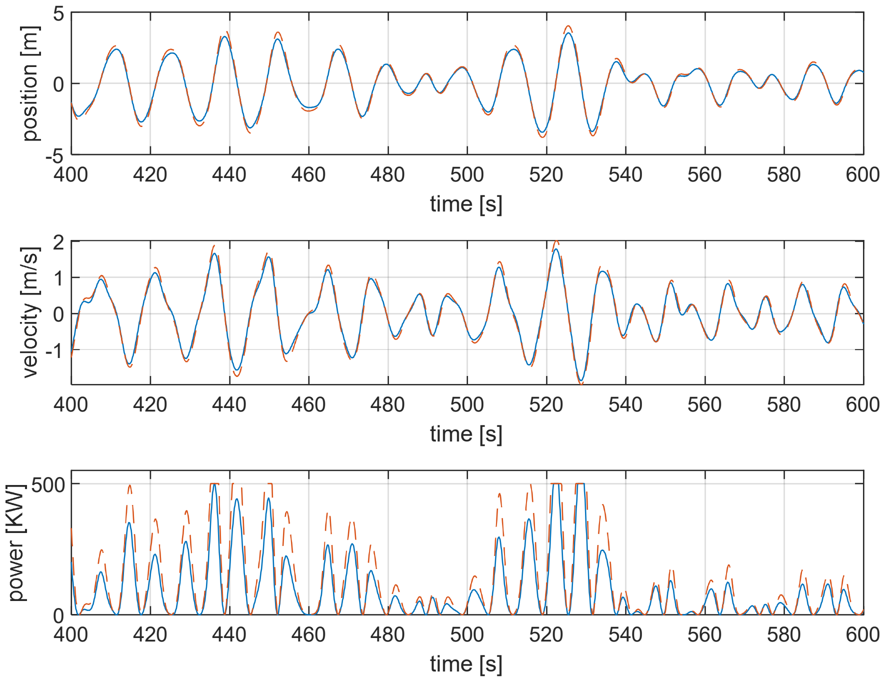

Fig. 13. Irregular sea state time series related to Hs=2.5 m and Tp = 14 s. Former CECO @180 kNs/m results and optimized CECO @270 kNs/m are depicted respectively by blue and red (dotted) lines.

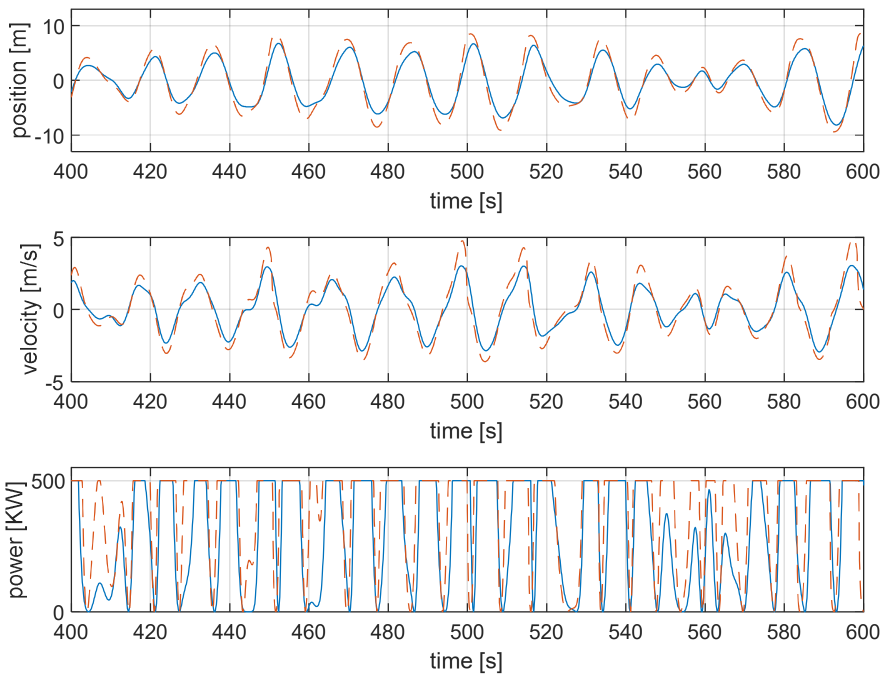

Fig. 14. Irregular sea state time series related to Hs = 7.5 m and Tp = 16 s. Results relative to former CECO @260 kNs/m and optimized CECO @400 kNs/m are depicted respectively by blue and red (dotted) lines.

5.3. Power matrixes and annual energy production

Results of the mean power output for all sea states considered are presented in the form of power matrices, respectively by using frequency-domain (Fig. 15) and time-domain (Fig. 16) models. For obtaining these power matrices the C_{pto} damping values were utilized, which were found from frequency-domain calculations [26]. Such C_{pto} values are based on the solution of the linearized fluid-structure interaction problem in the frequency-domain. It has to be pointed out that using a time-domain approach for finding the best C_{pto} values, as done in [48], may give improved results in terms of performances. However, the latter method was not used in the present study, as it may be more dependent on the sea spectrum considered and end-stops span length.

Fig. 15 and Fig. 16 display the power matrices relative to 45 sea states, for both CECO geometries with 30° of PTO inclination and the best PTO damping coefficients (Fig. 6, a). As can be observed frequency-domain power matrices have high values of mean power for high H_s. This result occurs because no generator rated power limit is considered. Overall, an evident better performance of the optimized geometry over the former design is observed for all the sea state conditions above 8 s of peak wave period T_p. Below that period, the former design performed only slightly better than the optimized geometry.

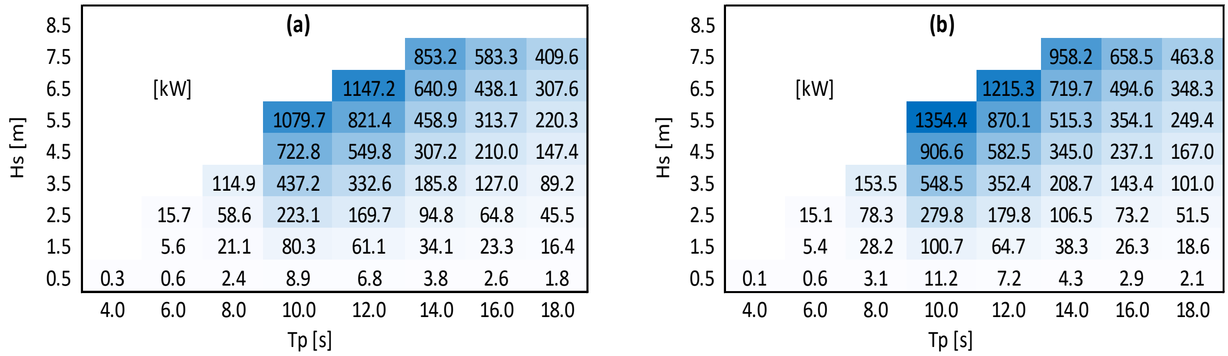

Fig. 15. CECO power matrix obtained with the frequency-domain model where no end-stops are considered and fixed damping values are used. (a) is relative to the former geometry @ 14.90 kN.s/m and (b) for the optimized geometry and (b) optimized CECO @ 23.13 kN.s/m.

For the former geometry, changing the rated power limit (from 0.5 to 1.5 MW) appears to only slightly affect the mean power output for sea states up to H_s= 3.5 m, Fig. 16 (a, c, e). In contrast, for the optimized geometry, higher-rated power limits appear to clearly and positively influence the average power produced (starting from sea states of H_s= 2.5 m), Fig. 16 (b, d, f).

(a) [kW]

Hs [m] \ Tp [s]	4.0	6.0	8.0	10.0	12.0	14.0	16.0	18.0
8.5								
7.5						276.7	234.9	208.9
6.5					280.8	251.2	205.8	179.0
5.5				216.6	257.6	216.9	170.1	143.9
4.5				196.9	224.4	172.1	128.1	105.9
3.5			124.3	162.3	174.5	118.8	84.1	67.9
2.5		58.7	68.0	118.3	106.5	64.1	44.0	35.1
1.5		21.3	24.6	54.3	40.5	23.2	15.9	12.7
0.5	2.1	2.4	2.7	7.2	4.5	2.6	1.8	1.4

(b) [kW]

Hs [m] \ Tp [s]	4.0	6.0	8.0	10.0	12.0	14.0	16.0	18.0
8.5								
7.5						313.5	277.0	251.9
6.5					313.4	290.6	250.6	223.7
5.5				294.5	293.1	260.0	217.4	188.6
4.5				274.7	262.6	218.7	174.4	146.2
3.5			141.6	236.3	213.3	162.1	122.0	98.9
2.5		56.1	80.1	174.7	140.7	94.6	67.5	53.2
1.5		20.4	29.4	82.8	56.9	34.9	24.5	19.3
0.5	1.1	2.3	3.3	9.9	6.4	3.9	2.7	2.1

(c) [kW]

Hs [m] \ Tp [s]	4.0	6.0	8.0	10.0	12.0	14.0	16.0	18.0
8.5								
7.5						412.6	320.6	267.5
6.5					422.2	351.5	262.0	215.4
5.5				271.0	366.7	279.7	200.7	162.4
4.5				236.4	296.1	201.2	139.9	111.9
3.5			133.2	178.6	206.7	125.4	85.8	68.4
2.5		58.7	68.3	122.0	111.4	64.3	44.0	35.1
1.5		21.3	24.6	54.4	40.5	23.2	15.9	12.7
0.5	2.1	2.4	2.7	7.2	4.5	2.6	1.8	1.4

(d) [kW]

Hs [m] \ Tp [s]	4.0	6.0	8.0	10.0	12.0	14.0	16.0	18.0
8.5								
7.5						501.8	416.6	357.5
6.5					504.8	444.3	355.9	297.8
5.5				446.8	453.9	370.2	284.8	232.8
4.5				394.7	378.6	282.4	208.1	166.0
3.5			155.9	311.3	274.1	185.4	131.8	103.7
2.5		56.2	81.2	202.0	155.5	96.8	68.0	53.3
1.5		20.4	29.4	84.7	57.0	34.9	24.5	19.3
0.5	1.1	2.3	3.3	9.9	6.4	3.9	2.7	2.1

(e) [kW]

Hs [m] \ Tp [s]	4.0	6.0	8.0	10.0	12.0	14.0	16.0	18.0
8.5								
7.5						480.3	354.0	286.2
6.5					495.1	394.6	280.1	224.0
5.5				281.2	414.5	299.4	207.1	164.8
4.5				241.7	320.3	206.0	140.8	111.9
3.5			133.6	179.0	213.3	125.6	85.8	68.4
2.5		58.7	68.3	122.0	111.6	64.3	44.0	35.1
1.5		21.3	24.6	54.4	40.5	23.2	15.9	12.7
0.5	2.1	2.4	2.7	7.2	4.5	2.6	1.8	1.4

(f) [kW]

Hs [m] \ Tp [s]	4.0	6.0	8.0	10.0	12.0	14.0	16.0	18.0
8.5								
7.5						621.6	491.8	406.4
6.5					629.2	528.3	403.5	327.1
5.5				523.0	545.1	421.0	309.8	245.5
4.5				443.4	432.5	303.2	215.5	169.9
3.5			157.2	333.0	293.8	188.7	132.7	103.8
2.5		56.2	81.2	207.8	157.4	96.8	68.0	53.3
1.5		20.4	29.4	84.7	57.0	34.9	24.5	19.3
0.5	1.1	2.3	3.3	9.9	6.4	3.9	2.7	2.1

Fig. 16. Power matrices of former CECO (left column) and optimized CECO (right column) calculated by considering rated power limits of 500 KW (a, b), 1MW (c, d) and 1.5 MW (e, f).

The power matrices were crossed with the wave resource matrix (Fig. 4) for estimating the annual energy production (AEP) for both geometries analysed. As expected, the AEP and the annual capture width ratio CWR (as def. in [49]) of the optimized CECO are significantly higher, Fig. 17**Error! Reference source not found.Error! Reference source not found.**. It is noticed that the AEP levels for the former CECO are similar for the three generator rated power values assessed, *i.e.* about 400 MWh/year. Differently, the increase of the generator rated power to 1 and 1.5 MW allows increasing the AEP for the optimized geometry up to about 620 MWh/year (1.5 MW case).

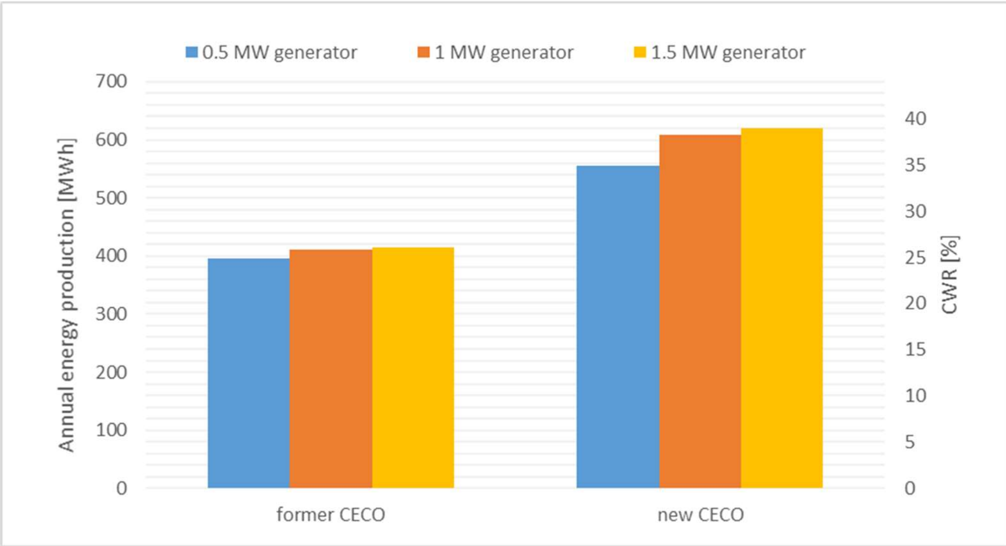

Fig. 17. Annual energy production (AEP) and capture width ratio (CWR) from former and optimized CECOs for different rated power values of the electrical generator.

5.4. General aspects

In Table 2, the former and the optimized CECO designs are compared in terms of indices relative to AEP per device mass and per surface area (both full and immersed surface areas of the LMMs) and power per root mean square (RMS) of PTO force. It can be noted that the former geometry has a higher energy per device mass ratio (for all generator rated power values considered). Similarly, the AEP per surface area is slightly higher for the former geometry. For the recurrent sea states (T_p = 10-14 s and H_s = 1.5-2.5 m), the power per RMS of PTO force appears to be similar between the two geometry. Differently, for the more severe sea state considered (T_p = 16 s, H_s = 7.5 m), the power per RMS of PTO force is markedly higher for the optimized geometry. These results may indicate that the optimized geometry would be more advantageous for more energetic sea states.

Table 2. Indices of former and optimized CECO comparison.

Performance index		**Former CECO**			**Optimized CECO**		
		Generator rated power (MW)					
		0.5	**1.0**	**1.5**	**0.5**	**1.0**	**1.5**
Energy per device's mass	[KWh/kg/year]	2.859	2.978	2.995	1.866	2.045	2.087
Energy per surface area	[MWh/m^2/year]	1.385	1.442	1.451	1.131	1.239	1.264
Energy per wetted surface area	[MWh/m^2/year]	2.414	2.514	2.528	1.936	2.121	2.164
Power per RMS of PTO force [W/N]	@ Tp=10 s, Hs=1.5 m		0.908			0.822	
	@ Tp=14 s, Hs=2.5 m		0.295			0.295	
	@ Tp=16 s, Hs=7.5 m		0.517			0.708	

Results also indicate that increasing the generator rated power value with the optimized geometry might allow rising the annual energy production, for instance by incrementing the rated power value from 0.5 to 1.5 MW about 12% more annual energy can be obtained (Table 2). This makes evident the importance of choosing the right generator size, based on a cost-benefit analysis because a larger generator might not be justifiable in economic terms. Additional work should be directed towards analysing the daily power output throughout a reference year and the costs of the electrical infrastructure including costs of generators aiming at selecting a suitable generator size. At such stage, it would be opportune to consider, as well, several devices in a realistic farm configuration.

Another important design factor that requires attention is the frame length, which determines stroke span between end-stops. To assess this parameter the positions of end-stops were varied. As can be observed inFig. 18, three different stroke span lengths are compared for the optimized CECO, respectively 7.5, 10.5 m and infinite case (unlimited). For the five most relevant sea states considered (of higher wave energy resource), it is noticed that higher efficiency η occurs at T_p=10 s. The stroke length appears to affect power production level, for the most, during cases relative to the sea states having T_p equal to 10 and 12 s. The stroke span length almost does not influences the power production level for sea states of T_p = 14 s. These results shall be interpreted taking into account that the natural period of tested CECO is 10 s.

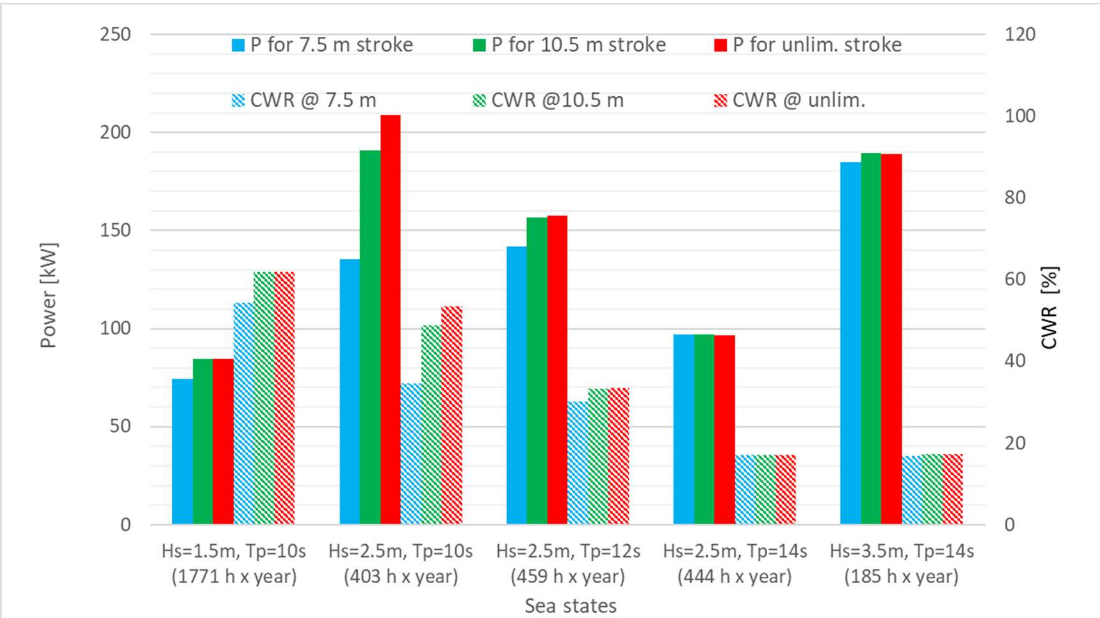

Fig. 18. Power and efficiency for the 5 most relevant sea states (optimized CECO). Here different translating frame stroke length were assessed (9, 12 m and unlimited).

6. Conclusions

A time-domain model of CECO wave energy converter was developed and used to assess the optimized geometry (slender shape) of the lateral mobile modules against the former one (half-cylinder shape). The model allowed analysing CECO performance taking into account realistic irregular sea states (relative to a reference offshore site), as well, evaluating different generator rated power limits and permitted the inclusion of end-stops to realistically limit motion amplitude.

Clearly, for the recurrent sea states, the optimized geometry allows more energy to be produced from waves compared to the former one (between 160 and 200 MWh/year of additional energy). It was observed that the annual energy production of CECO could be further increased if a generator with a higher rated power is used. For instance, the optimized geometry can allow a rise of the annual energy production of about 10% if a 1.5 MW rated generator is used instead of a 0.5 MW one. The selection of the generator should hence be based on a techno-economic assessment that takes into account its cost and the revenue associated with the energy production.

The stroke span was shown to be a key factor affecting CECO efficiency and energy production. For the optimized geometry, it was found that a relatively short stroke span (7.5 m) significantly reduces the mean power production. In fact, for sea states of T_p=10 s (resonant frequency of the tested CECO unit), a 30 % reduction of the mean power output is observed. Differently, a short span little affects the mean power production for sea states of T_p=14 s. In the future, PTO control strategies could be implemented to limit the amplitude of CECO excursions near its resonant period.

Despite the evident advantages of the new geometry in terms of energy production, further studies addressing, *e.g.* generator sizing, maintenance costs, structural loads and control strategies are required to further develop CECO and assess accurately the potential economic advantages given by choosing the optimized geometry.

Acknowledgements

The authors would like also to thank the support from: the Project OPWEC - POCI-01-0145-FEDER-016882 and PTDC/MAR-TEC/6984/2014, funded/co-funded by FEDER through COMPETE 2020 – Programa Operacional Competitividade e Internacionalização (POCI) and by Portuguese national funds, through the FCT - Fundação para a Ciência e a Tecnologia, IP; and the project PORTOS – Ports Towards Energy Self-Sufficiency (EAPA 784/2018), co-financed by the Interreg Atlantic Area Programme through the European Regional Development Fund. Furthermore, during this work, V. Ramos has been supported by the program of Stimulus of Scientific

Employment Individual Support (CEECIND/03665/2018) from the Portuguese Foundation for Science and Technology (FCT).

References

1. Cruz, J. "Ocean Wave Energy Current Status and Future Perspectives", ed. Springer. 2008: Cambridge University Press, 2008.
2. Falcão, A. F. d. O. "Wave energy utilization: A review of the technologies". *Ren. and Sust. Energy Rev.*, **2010**, 10.1016/j.rser.2009.11.003.
3. Marinhero, J., Rosa-Santos, P., Taveira-Pinto, F., and Ribeiro, J. "Feasibility study of the CECO wave energy converter", in *Maritime Technology and Engineering*, Editor, C.T.a.F. Group). 2014 (2014). p. 1259-1267. ISBN 978-1-138-02727-5, 10.1201/b17494-170.
4. Wave Star, A/S. http://wavestarenergy.com/, 2000 [accessed 20 Jan. 2020].
5. Eco Wave Power. https://www.ecowavepower.com/, 2020 [accessed 15 June 2020].
6. Coiro, D. T., G.; Calise, G.; Bizzarrini, N. "Experimental test and numerical shape optimization of a point pivoted absorber for wave energy conversion ". In *Proceedings of the VI International Conference on Computational Methods in Marine Engineering MARINE*. 2015.
7. Belfast, Q. s. U. o. "ISLAY LIMPET WAVE POWER PLANT ". 2002. Available from: https://tethys.pnnl.gov/sites/default/files/publications/Islay_LIMPET_Report.pdf (accessed on 26/06/2020).
8. Falcão, A. F. O., Sarmento, A. J. N. A., Gato, L. M. C., and Brito-Melo, A. "The Pico OWC wave power plant: Its lifetime from conception to closure 1986–2018". *Applied Ocean Research*, **2020**. 98: 102104, ISSN 0141-1187, 10.1016/j.apor.2020.102104.
9. Mehlum, E. "TAPCHAN. In: Evans D.V., Falcão A.F.O. (eds) Hydrodynamics of Ocean Wave-Energy Utilization". In *Proceedings of the International Union of Theoretical and Applied Mechanics*. Springer, Berlin, Heidelberg, ISBN/ISSN 978-3-642-82668-9, https://doi.org/10.1007/978-3-642-82666-5_3.
10. Margheritini, L., Vicinanza, D., and Frigaard, P. "SSG wave energy converter: Design, reliability and hydraulic performance of an innovative overtopping device". *Renewable Energy*, **2009**. 34(5): 1371-1380, ISSN 0960-1481, 10.1016/j.renene.2008.09.009.
11. Salter, S. H. "The Solo Duck". 1982. Available from: http://www.homepages.ed.ac.uk/v1ewaveg/0-Archive/EWPP%20archive/1982%20EWPP%20The%20Solo%20Duck.pdf (accessed on 1/12/2019).
12. SEABASED GROUP. https://www.seabased.com/, 2020
13. Archimedes Waveswing Submerged Wave Power Buoy (AWS) http://www.awsocean.com/archimedes-waveswing.html, 2020 [accessed 15 June 2020].
14. CETO. https://www.carnegiece.com/technology/, 2020 [accessed 15/06/2020].
15. Ocean Power Technology (OPT). https://www.carnegiece.com/technology/, 2020 [accessed 15 June 2020].
16. Osawa, H., Washio, Y., Ogata, T., Tsuritani, Y., and Nagata, Y. "The Offshore Floating Type Wave Power Device ”Mighty Whale” Open Sea TestsPerformance of The Prototype –", in *The Twelfth International Offshore and Polar*

Engineering Conference, International Society of Offshore and Polar Engineers: Kitakyushu, Japan.2002; p. 6.

17. Babarit, A., Clément, A., Ruer, J., and Tartivel, C. "SEAREV: A fully integrated wave energy converter". **2006**.
18. Mattiazzo, G. "State of the Art and Perspectives of Wave Energy in the Mediterranean Sea: Backstage of ISWEC". **2019**, 10.3389/fenrg.2019.00114.
19. Boren, B. C., Batten, B. A., and Paasch, R. K. "Active control of a vertical axis pendulum wave energy converter". In *Proceedings of the 2014 American Control Conference*. 2014. ISBN/ISSN 2378-5861, 10.1109/ACC.2014.6859459.
20. Kofoed, J. P., Frigaard, P., Friis-Madsen, E., and Sørensen, H. C. "Prototype testing of the wave energy converter wave dragon". *Renewable Energy*, **2006**. 31(2): 181-189, ISSN 0960-1481, 10.1016/j.renene.2005.09.005.
21. AW-Energy. https://aw-energy.com/waveroller/, 2020 [accessed 16/06/2020].
22. Henry, A., Doherty, K., Cameron, L., Whittaker, T., and Doherty, R. "Advances in the Design of the Oyster Wave Energy Converter". 2010, 2010.
23. Rosa-Santos, P., Taveira-Pinto, F., Rodríguez, C. A., Ramos, V., and López, M. "The CECO wave energy converter: Recent developments". *Ren. Energy*, **2019**. 139: 368-384, ISSN 0960-1481, 10.1016/j.renene.2019.02.081.
24. Pecher, A. and Kofoed, J. P. "Handbook of Ocean Wave Energy". 2017: Springer, Cham, 2017. ISBN 978-3-319-39888-4, 10.1007/978-3-319-39889-1.
25. Todalshaug, J. H., Ásgeirsson, G. S., Hjálmarsson, E., Maillet, J., Möller, P., Pires, P., Guérinel, M., and Lopes, M. "Tank testing of an inherently phase-controlled wave energy converter". *International Journal of Marine Energy*, **2016**. 15: 68-84, ISSN 2214-1669, 10.1016/j.ijome.2016.04.007.
26. Rodríguez, C. A., Rosa-Santos, P., and Taveira-Pinto, F. "Hydrodynamic optimization of the geometry of a sloped-motion wave energy converter". *Ocean Engineering*, **2020**. 199: 107046, ISSN 0029-8018, https://doi.org/10.1016/j.oceaneng.2020.107046.
27. Salter, S. H. and Lin, C. "The Sloped IPS Wave Energy Converter". In *Proceedings of the 2nd European Wave and Tidal Energy Conf.* 1995. Lisbon.
28. López, M., Ramos, V., Rosa-Santos, P., and Taveira-Pinto, F. "Effects of the PTO inclination on the performance of the CECO wave energy converter". *Marine Struct.*, **2018**. 61: 452-466, 10.1016/j.marstruc.2018.06.016.
29. Ramos, V., López, M., Taveira-Pinto, F., and Rosa-Santos, P. "Performance assessment of the CECO wave energy converter: Water depth influence". *Ren. Energy*, **2018**: 341-356, 10.1016/j.renene.2017.10.064.
30. Ramos, V., Lopez, M., Taveira-Pinto, F., and Rosa-Santos, P. "Influence of the wave climate seasonality on the performance of a wave energy converter: A case study". **2017**: 303-316, 10.1016/j.energy.2017.06.080.
31. Davidson, J. and Costello, R. "Efficient Nonlinear Hydrodynamic Models for Wave Energy Converter Design—A Scoping Study". *Journal of Marine Science and Engineering*, **2020**. 8(1), ISSN 2077-1312, 10.3390/jmse8010035.
32. Cummins, W. E. "The impulse response function and ship motions". *Schiffstechnic*, **1962**: 101–109.
33. ANSYS "Aqwa Reference Manual". Canonsburg, 2017. Available from: https://ansyshelp.ansys.com/ (accessed on 15/11/2019).
34. Rosa-Santos, P., Taveira-Pinto, F., Teixeira, L., and Ribeiro, J. "CECO wave energy converter: Experimental proof of concept". *Journal of Renewable and Sustainable Energy*, **2015**. 7(6): 061704, 10.1063/1.4938179.

35. Rodríguez, C. A., Rosa-Santos, P., and Taveira-Pinto, F. "Assessment of damping coefficients of power take-off systems of wave energy converters: A hybrid approach". *Energy*, **2019**. 169: 1022-1038, ISSN 0360-5442, 10.1016/j.energy.2018.12.081.
36. Rodríguez, C. A., Rosa-Santos, P., and Taveira-Pinto, F. "Experimental Assessment of the Performance of CECO Wave Energy Converter in Irregular Waves". *Journal of Offshore Mechanics and Arctic Engineering*, **2019**. 141(4), ISSN 0892-7219, 10.1115/1.4043177.
37. Booij, N., Ris, R., and Holthuijsen, L. "A third-generation wave model for coastal regions, Part I, Model description and validation". *J. Geophys. Res.*, **1999**. 104: 7649-7656.
38. Booij, N., Ris, R., and Holthuijsen, L. "A third-generation wave model for coastal regions, part II: verification". *J. Geophys. Res.*, **1999**. 104.
39. Jacob, D. and Podzun, R. "Sensitivity studies with the regional climate model REMO". *Meteorology and Atmospheric Physics*, **1997**. 63(1): 119-129, ISSN 1436-5065, 10.1007/BF01025368.
40. Group, T. W. "The WAM Model—A Third Generation Ocean Wave Prediction Model". *Journal of Physical Oceanography*, **1988**. 18(12): 1775-1810, ISSN 0022-3670, 10.1175/1520-0485(1988)018<1775:Twmtgo>2.0.Co;2.
41. Sarpkaya, T. S. "Wave Forces on Offshore Structures". 2010, Cambridge: Cambridge University Press, 2010. ISBN 9780521896252, https://doi.org/10.1017/CBO9781139195898.
42. Ursell, F. "Two-Dimensional Problems in Hydrodynamics and Aerodynamics. By L. SEDOV. John Wiley, 1965. 427 pp. 126s". *Journal of Fluid Mechanics*, **1965**. 22(4): 828-828, ISSN 0022-1120, 10.1017/S0022112065211179.
43. "WAMIT® - The state of the art in wave interaction analysis". 2019. Available from: http://www.wamit.com/index.htm (accessed on 1/12/2019).
44. Falnes, J. "Ocean Waves and Oscillating Systems". 2002: Cambridge University Press, 2002.
45. Wheeler, J. D. "Method for Calculating Forces Produced by Irregular Waves". *Journal of Petroleum Technology*, **1970**. 22(03): 359-367, ISSN 0149-2136, 10.2118/2712-PA.
46. Morison, J. R., Johnson, J. W., and Schaaf, S. A. "The Force Exerted by Surface Waves on Piles". *Journal of Petroleum Technology*, **1950**. 2(05): 149-154, ISSN 0149-2136, 10.2118/950149-G.
47. ANSYS "Aqwa Theory Manual". Canonsburg, 2015. Available from: https://ansyshelp.ansys.com/ (accessed on 22/03/2018).
48. Giannini, G., Rosa-Santos, P., Ramos, V., and Taveira-Pinto, F. "On the Development of an Offshore Version of the CECO Wave Energy Converter". *Energies*, **2020**. 13(5), ISSN 1996-1073, 10.3390/en13051036.
49. Babarit, A. "A database of capture width ratio of wave energy converters". *Ren. Energy*, **2015**. 80: 610-628, ISSN 0960-1481, https://doi.org/10.1016/j.renene.2015.02.049.